Available online at www.sciencedirect.com

jmr&t
Journal of Materials Research and Technology
www.jmrt.com.br

Original Article

The cathodic electrolytic plasma hardening of the 20Cr2Ni4A chromium-nickel steel

Bauyrzhan K. Rakhadilov[a], *Vladimir V. Buranich*[b,*], *Zarina A. Satbayeva*[a], *Zhuldyz B. Sagdoldina*[a], *Rauan S. Kozhanova*[a], *Alexander D. Pogrebnjak*[b,c]

[a] *Sarsen Amanzholov East-Kazakhstan State University, Ust-Kamenogorsk, Kazakhstan*
[b] *Sumy State University, 2, Rimsky Korsakov Str., 40007 Sumy, Ukraine*
[c] *D. Serikbaev East Kazakhstan State Technical University, Ust-Kamenogorsk, Kazakhstan*

ARTICLE INFO

Article history:
Received 24 March 2020
Accepted 7 May 2020
Available online 8 June 2020

Keywords:
Plasma-electrolytic hardening
20Cr2Ni4A steel
Heat treatment
Hardness
Wear

ABSTRACT

In order to obtain the modified surface structure of the 20Cr2Ni4A steel plasma electrolytic hardening (PEH) method was used. The surface hardening process was conducted in the aqueous electrolyte solution of 20% sodium carbonate and 20% urea. The sample consists of a ferritic-pearlitic structure, i.e. the part retains its viscous core, and the surface layer contains carbide particles. Hardening process induces martensite transformation and creation of carbide particles in the surface layer. The presence of carbide particles in the surface layers has a positive effect on the tribo-mechanical performance. Hardened structure 600 μm long was obtained with hardness increase up to 520 HV and 2.5 times higher wear resistance. Tribological test results showed the difference of the coefficient of friction as a function of surface roughness determined by plasma-electrolytic hardening process.

1. Introduction

Often the performance of machines and mechanisms depends on the wear resistance of parts, gears, shafts, internal combustion engines, and other friction joint parts. To increase durability, parts must have high strength and hardness of the surface layer. There many different techniques used to achieve this, such as carburizing, nitriding, flame hardening, induction and laser heat treatments [1].

Use of plasma-electrolytic treatment for surface hardening is a new approach, which has been recently introduced into the industry. The main advantages of this method are: high efficiency, significant depth of hardening (10 μm–10 mm), possible fulfillment with simple and cheap equipment. It presents an attractive and flexible process for technical applications due to the lack of restrictions on the size and geometric shape of the workpiece, shorter processing time, less environmental impact at lower temperatures compared to conventional plasma processes [2–6].

Surface hardening is achieved due to short-term (2–10 s) heating of the steel to the hardening temperature and subsequent rapid cooling. In this case, the heating rate should be high enough so that the heat does not have time to spread deep into the part and the volumetric hardening process does not occur [7].

Cathodic plasma electrolytic hardening (PEH) allows quick heat and gives opportunity to adjust the depth of the hardened layer directly. PEH method provides high-strength modified layers due to the high cooling rate. This is ensured by the

* *Corresponding author.*
E-mail: v.buranich@phe.sudmdu.edu.ua (V.V. Buranich).
https://doi.org/10.1016/j.jmrt.2020.05.020

Table 1 – The chemical composition of 20Cr2Ni4A steel.

Element	Fe	C	Si	Mn	Cr	Ni	S	P	Cu
Concentration at. %	93.16–94.87	0.16–0.22	0.17–0.37	0.3–0.6	1.25–1.65	3.25–3.65	Below 0.025	Below 0.025	Below 0.3

fact that the treatment process is carried out in an electrolyte based on a carbon-containing aqueous solution [8–11].

This article is dedicated to the study of the effect of hardening process on the structure and properties of steel that typically used in parts/tools fabrication. 20Cr2Ni4A structural Cr-Ni alloy steel is widely distributed in gears, wheels and their rims fabrication, as well as other heavy-duty parts [12,13]. 20Cr2Ni4A steel is practically not hardened in the traditional way. This type of steel is carburized or nitrocarburized, and then only heat treated [14]. PEH allows to obtain hardened surface layers of such low-carbon steels, without additional heat treatment. With rapid heat, which helps to obtain a thinner structure of processed steel it's become possible to obtain a more favorable combination of strength and toughness properties because of dynamic recrystallization [15,16].

The heating rate has a significant effect on the recrystallized grain size. Increase in kinetic energy leads to an increase in the amount of the recrystallization centers that forces grains grinding. The short-term dwelling of steel in the area of quenching temperatures and phase transitions at temperatures exceeding the equilibrium, lead to mechanical properties that differ from the properties of steel, hardened with traditional heat sources [1,17]. In this regard, the study of the changes in the structure and tribomechanical properties of the 20Cr2Ni4A steel, after cathodic electrolytic plasma hardening is of great scientific and practical interest.

2. Materials and methods

As a sample for research, structural alloying steel 20Cr2Ni4A was selected. Material choice was inspired due to widespread of this type of steel in gears, wheels and rims manufacturing, that is usually appears in many kinds of mechanical engineering. Samples were cut in the parallelepiped form with linear dimensions of $15 \times 15 \times 10\,mm^3$ from a bar pre-hardened at 780–820 °C (factory conditions). Table 1 presents the chemical composition of this grade of steel.

Cathodic PEH conducted at Research Center "Surface Engineering and Tribology" of S. Amanzholov East Kazakhstan State University on UEPOM-M technological system (Fig. 1). The installation consists of a chamber for electrolyte-plasma processing of materials, a personal computer and a power supply capacity of 40 kW.

The EPT process of steel samples is as follows. Before starting the working bath (8) is filled with the electrolyte. The electrolyte with the help of a pump (6) installed at the bottom of the working bath, enters the electrolytic cell (4). In this case, the electrolyte exits through the hole of the conical partition (3) in the form of a jet and fills the electrolytic cell. Then, the electrolyte is merged over the edge of the electrolytic cell into a pallet (5), and then back into the working bath. Thus, the electrolyte is in a circulating mode with a flow rate of 4–7 l/min, where the flow rate of cooling water into the heat exchanger (7) is 3–6 l/min. The established cooling parameters maintain the temperature in the range of 40–70 °C during heating the samples to a temperature of 800–900 °C. The sample was fastened to the clamping device so that its depth of immersion in the electrolyte was corresponded to the processed zone of the 2–3 mm from the inlet of the conical partition. At the same time, through the inlet of the cone-shaped partition, which is 10–15 mm lower than the height of the electrolytic cell, an electrolyte stream lends itself to the treatment area. Then the anode (2) is connected to the positive pole of the power source, and the workpiece (cathode) (1) to its negative pole.

Process of plasma electrolytic treatment was carried out in 20% sodium carbonate +20% urea aqueous solution at following regime: the applied voltage −320 V with current density

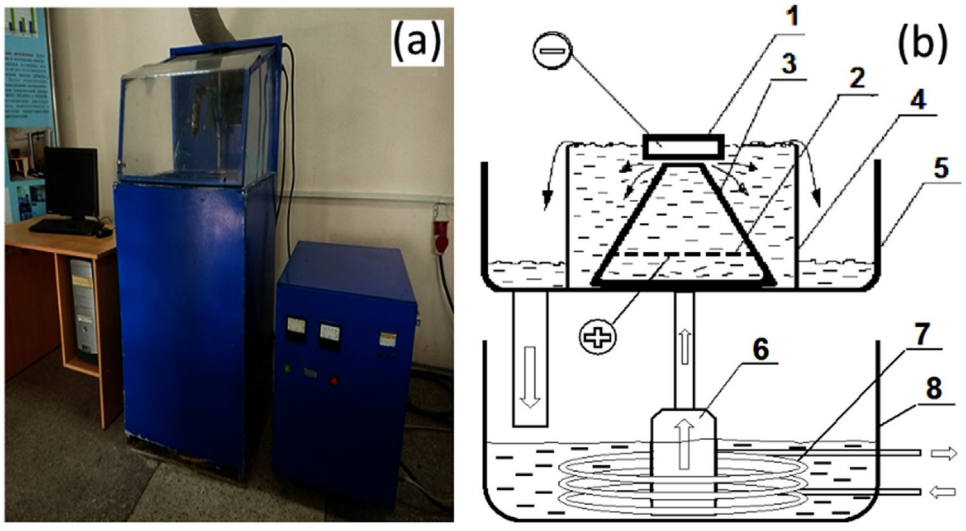

Fig. 1 – Overview (a) and scheme (b) of UEPOM-M EPT system: 1 – processed sample (cathode), 2 – stainless steel anode, 3 – cone-shaped partition, 4 – electrolytic cell, 5 – pallet, 6 – pump, 7 – heat exchanger, 8 – bath with electrolyte.

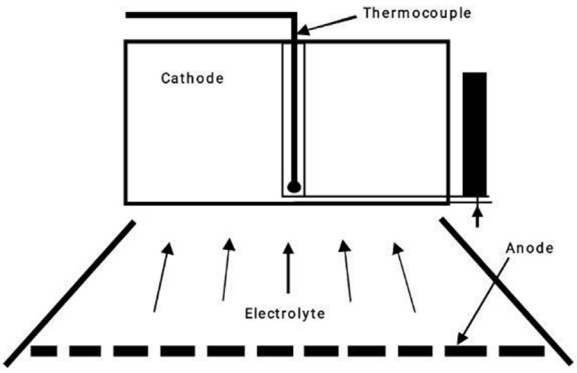

Fig. 2 – Scheme representing the position of the thermocouple in a sample during temperature measuring.

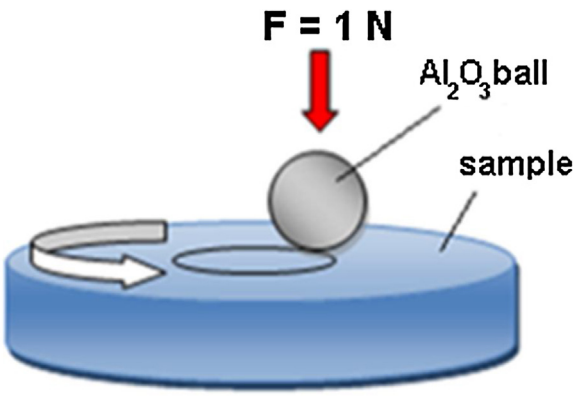

Fig. 3 – Scheme of ball-on-disk tribological test.

of 25 A/cm^2, plasma exposure time counted from the applying the current 2 s. The electrolyte was stirred with an air pump, its nozzle located on the bottom of the working chamber under the sample. In this regime, the samples were heated up to ~850–900 °C. Cooling was carried out in a flowing electrolyte after turning the voltage off.

The heating temperature of the studied sample was measured using a digital multimeter UNIT-33C and chromel-alumel thermocouple (accuracy 2% in the range of 40–1000 °C). Thermocouple was inserted into a hole drilled in a cathode at a distance of 2 mm from heated surface. The layout of the thermocouple is shown in Fig. 2.

An optical microscope ALTAMI-MET-1M was used for investigation of the sample surface. To identify the microstructure, chemical etching of thin sections in a 4% alcohol nitric acid solution was applied (etching time 10–15 s). Before and after the processing to characterize the morphology and atomic composition, surface was examined by scanning electron microscope (JSM-6390LV) with mounted energy-dispersive microanalyzer (INCAEnergy).

Phase and structure analysis derived from XRD patterns obtained on X'PertPro diffractometer in Cu-Kα radiation (40 keV, at a rate of 0.02°/s). Mechanical properties defined by PMT-3 M microhardness tester under constant load of 0.1 kg and 10 s exposure time.

Tribological tests performed on high temperature tribometer THT-S-BE-0000 (Tomsk Materials Science Center) by standard ball-on-disk method (ASTM G 133-95 and ASTM G 99 [18]). Test setup schematically shown in Fig. 3.

An Al_2O_3 ball 6 mm in diameter was used as a counterbody. Tests carried out at 1 N normal load and linear velocity of 2 cm/s, with a wear curvature radius of 5 mm. The total sliding distance reached 31.4 m, that's enough for wear testing of the hardened layer. Wear tracks were investigated using a non-contact 3D profilometer MICROMEASURE 3D station.

3. Results and discussion

3.1. *Plasma electrolytic discharge*

The gaseous envelope around the cathode can be produced by the different chemical reactions. Reaction in aqueous solution accompanied by dissolving of urea and creating of natrium cyanide, carbon oxide, ammonium and mostly water. In the mentioned above aqueous solution Na^+, CO^-, OH^-, H^+ ions are formed. Negatively charged ions give away excess electrons, when passing through the holes of the anode, and cations recombine on the surface of the cathode (steel part) [17].

The most likely processes under following experimental conditions may be expressed in following reactions [19,20]:

$$2H + 2e^- \rightarrow H_2 \quad (1)$$

$$CO(NH_2)_2 \rightarrow NH_3 + HNCO \quad (2)$$

$$NHCO + H_2O \rightarrow NH_3 + CO_2 \quad (3)$$

$$HCONH_2 \rightarrow NH_3 + CO \quad (4)$$

To illustrate electrical field and temperature behavior between surfaces of the liquid electrode and sample a volt-current and exposure time-temperature characteristics were measured (Fig. 4).

From the shape and curvature of trend-line, four areas can be distinguished [3,7]. The first region, in which the magnitude of the current is proportional to the applied voltage from 60 to 140 V. Electrolyte washes the cathode surface. The electrolyte temperature on the cathode surface is beneath boiling point. In the range of 145–160 V at cathode surface a thin gaseous vapor layer is appeared, which reduces the current with increasing voltage [21–23]. Third area (160–260 V) characterized by instability of the system due to the rapid boiling of the electrolyte and individual discharges at different points of the active electrode. At the same time, a gas-vapor shell with a thickness of about 50–120 μm is created near the surface of the active electrode, which isolates the active electrode from the electrolyte. The absence of bubble boiling and a sharp drop of current determine the third region, due to the fact that the resulting gas-vapor shell has a greater electrical resistance than liquid electrolyte. Since the gas-steam shell is less electrically conductive, the main voltage drop occurs precisely in this zone, where more heat is released. Due to the formation of a gas-vapor shell and passage of electric current through it, a low-temperature plasma is formed. With a further increase in voltage to 260–320 V, an abnormal discharge is

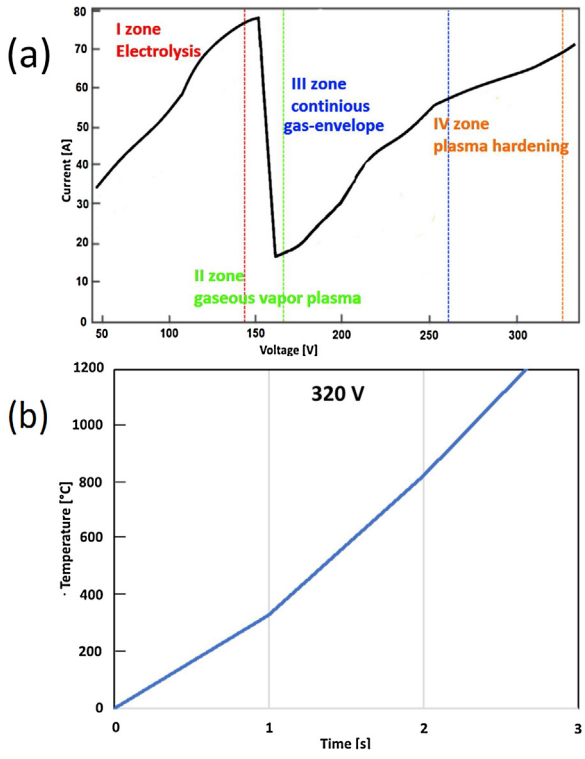

Fig. 4 – Current-voltage characteristic (a) and temperature versus plasma curve (b) of cathodic plasma electrolytic discharge for aqueous solution of 20% Na_2CO_3 + 20% urea.

formed, which leads to a more rapid increase in current and temperature of the electrode up to its point of melting (fourth area). Thus, in this branch of characteristic we can observe a region that can be used for plasma hardening, characterized by stable intense combustion of an anomalous discharge, since a plasma surface hardening requires a strong plasma exposure, which allows the parts to heat up at a high speed. As we can see from the temperature dependence of this electrolyte composition, it is more than enough for fast heating and, as a consequence, high-quality surface hardening.

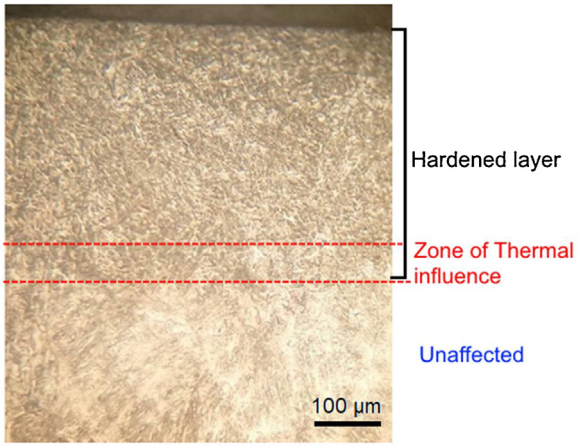

Fig. 6 – Optical microstructure of the PEH processed 20Cr2Ni4A cross section.

3.2. *Microscopy studies*

Within given hardening conditions a treated steel sample with modified structure has been obtained. SEM surface images (Fig. 5) illustrate aftereffects of cathodic plasma processes. Fast thermal diffusion-less transformations in the grain-boundary sites of fragmented ferrite accompanied by formation of visible cementite (Fe_3C) and martensite phases. Metallographic analysis showed that 20Cr2Ni4A steel in the initial state consists of a ferrite-pearlite structure. The total volume of pearlite fragments was ~10%. The average grain size of ferrite around 100 μm. Martensitic structure is formed after the CEPH, decomposition of pure-iron particles is quite observable.

Fig. 6 presents an optical micrograph of the cross section of processed sample. It can be seen that the fragment of the surface layer has a fine-grained structure, passing to a larger structure of the intermediate layer and further to the metallic base. The thickness of the modified layer is approximately 600–650 μm. The obtained microstructure can be divided into 3 parts: 1 – zone of intense structural transformations that contain hardened layer; 2 – heat affected (transition) zone; 3 – zone with the original ferrite matrix structure (base).

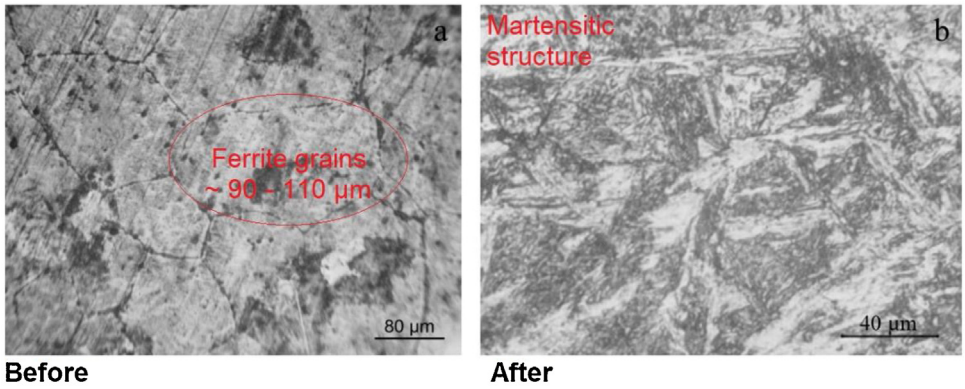

Fig. 5 – Microstructure of the steel surface before and after PEH.

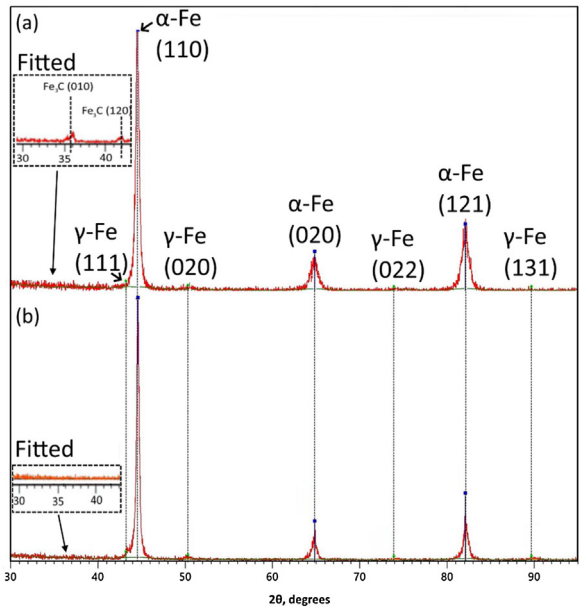

Fig. 7 – Comparison of x-ray diffraction (XRD) patterns after (a) and before (b) PEH treatment.

3.3. *Structural and compositional analyses*

Fig. 7 shows the X-ray diffraction patterns that illustrate the structural evolution of the PEH treated steel sample. Mainly both XRD patterns consist of ferrite (α-Fe) peaks. Gamma-Fe (austenite) was present in small fractions in the processed and initial steel and its intensity of the (111) reflection was decreased after PEH as a result of the martensitic transformation to body centered tetragonal lattice. This type of transformation must be induced by high temperature and surficial carbon saturation. Low intensity cementite (Fe_3C) reflexes of (101) and (120) planes were detected at the hardened surface layer (Fig. 7 inset). Ferrite phase peaks shifted to lower angles with lattice parameter $a_{\alpha\text{-Fe}}$ increase from 2.8153 Å to 2.8395 Å. Thus, volume expanded as consequence of Fe to Fe_3C partial transition. distortion is most likely because of the martensite particles that was observed by SEM analysis (Fig. 5). Usually martensite has several diffraction angles depending on the diffracting crystallographic planes that are close to those of ferrite, but are broader. In our case presence of martensite particles also confirmed by the intensity and a broadness increase of the (110), (020) and (121) peaks. An increase in the intensity of α-Fe structural peaks also corresponds to their decomposition caused by internal stresses due fast-thermal processes. Broadening and shift of α phase diffraction lines indicates to the generation of additional amount of vacancies and dislocations at the processed surface area. Grain size of α-Fe particles calculated by Scherrer formula decreased from 26 ± 4.7 to 19 ± 4.2 nm.

The changes in the elemental composition of the surface derived from EDS shown in Fig. 8. After thermal processes bright crystals of carbide particles are visible on the surface of the treated steel. However, the EDS spectrum, however, shows insignificant changes in the elemental composition of the material surface. The atomic percentage of carbon increased only by 1%. The most probable carbon source may be carbon monoxide, which is formed by the decomposition of triethanolamine, formamide or urea [19,24,25]. The absorption process can be represented as:

$$2CO \rightleftarrows CO_2 + C(\gamma\text{-Fe}(C)) \quad (5)$$

3.4. *Wear and tribology tests*

The microhardness values (Fig. 9) of treated surface layer is much higher than that of initial up to 2.5–3 mm in depth along the sample. The average values of the carburized layer 515–520 $HV_{0.2}$. The high HV pointed cementite and martensite phases formation in the surface layer [26]. The transition zone pattern has a flowing transition from the hardened layer to the base, while the microhardness of the transition zone is slightly less than the base, and the microhardness of the ferrite base does not change.

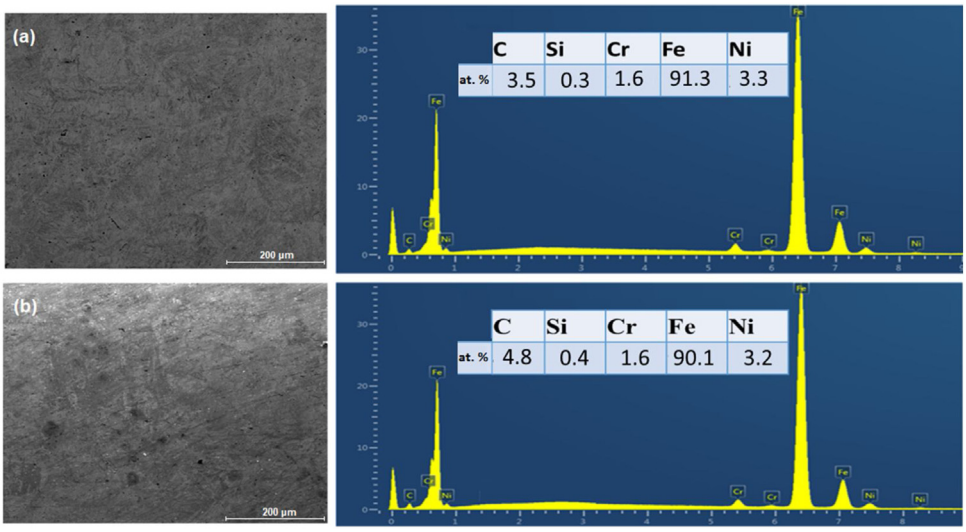

Fig. 8 – SEM images with EDS analysis. Initial steel 20Cr2Ni4A surface (a), after PEH (b).

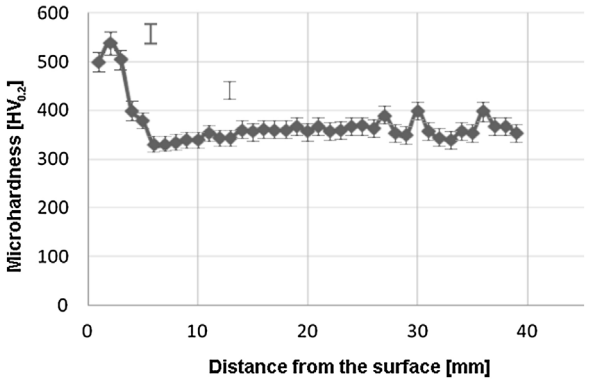

Fig. 9 – Microhardness distribution along the depth of the hardened sample.

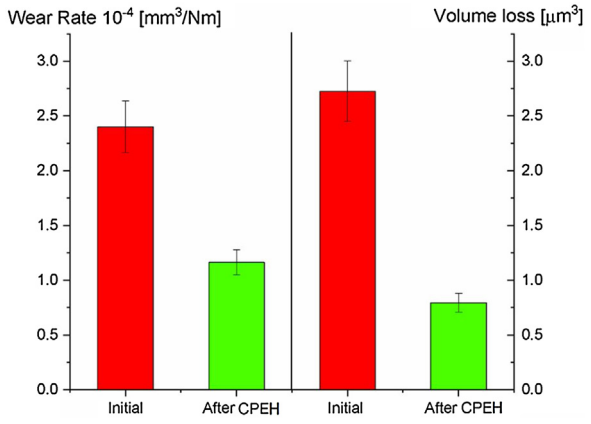

Fig. 10 – Comparison of wear rate and wear volume loss of 20Cr2Ni4A steel before and after hardening process.

Tribological properties of the modified layer were characterized by wear rate and coefficient of friction. Fig. 10 shows the results of "ball-on-disk" tests. The calculated value of wear rate for hardened steel amounted to 1.16×10^{-4} mm^3/Nm along with 0.794 μm^3 of volume loss which was 2–2.5 lower compared to the initial steel.

Images of the wear tracks after tests have taken with a 3D profilometer (Fig. 11). In both of cases we observe abrasive wear model. Abrasive wear caused by abrasive particles such as dust from work environment due to experimental conditions. The "plowing" effect after CEPH is significantly less

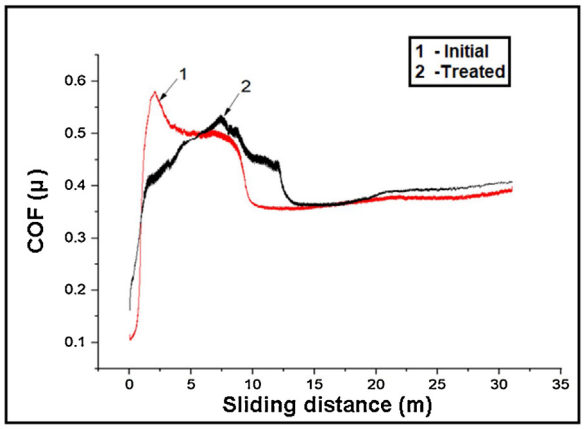

Fig. 12 – Graphs showing the friction coefficient (μ) as a function of sliding distance.

compared to the untreated sample assessing the geometrical parameters of the wear tracks [27].

Cathodic-plasma processes known as boosting of the surface roughness unlike the anodic [28]. High voltage between the electrodes leads to concentration of positive ions that are present in the electrolyte, in the close proximity of the cathode, mostly on the surface with producing of gas bubbles (H_2 mostly). Kinetic force impact on the surface is highly affected by the presence of positive ions at negative voltages. After reaching enough kinetic energy plasma bubbles explodes and create the micro-craters on the surface [23]. The thermal processes are also affected the roughness of treated sample, but at applied DC voltage of −320 V heat process runs almost linearly due specifics of arc-plasma discharge [13]. Even due the fact that process occurs very fast (2 s) it caused visible microcraters and spheroids on the surface. Hence mechanism and value of coefficient of friction must change. Fig. 12 shows friction behavior during tribological test. Consuming that counterbody and the surface was way more different materials and it also caused an abrasive wear process with lots of short grooves and debris generated by plastic deformation of contacting surfaces. It's reasonable to consider that pop-up in the values of the friction coefficient of hardened sample is related to the sliding on the thin grooves placed parallel due intense interaction with wear debris [27,29,30]. After sliding distance of

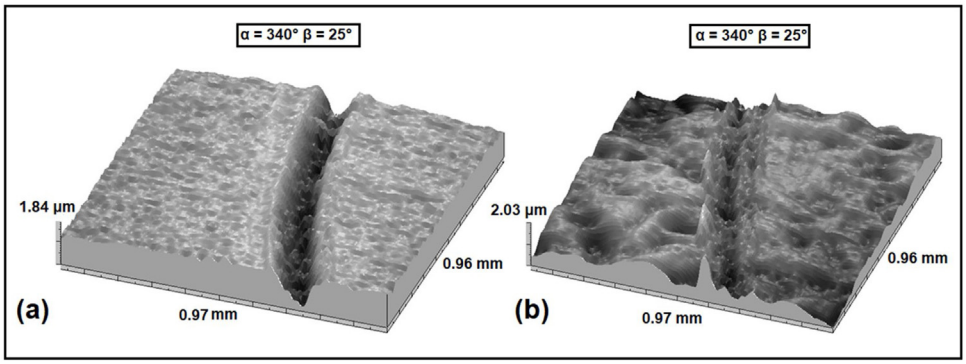

Fig. 11 – Image of a fragment of the wear track of the initial (a) and PEH treated (b) 20Cr2Ni4A steel sample.

15 m difference between the friction force of treated and initial sample almost imperceptible.

4. Conclusion

During this work cathodic plasma electrolysis hardened 20Cr2Ni4A steel sample was investigated:

1. Metallographic analysis proved fragmentation of the ferrite particles and formation of the needle-like martensitic formations on the surface of the 20Cr2Ni4A steel by plasma electrolytic hardening. SEM-EDS and XRD analyses revealed that the surface layer structure consists of the martensitic mixture with a low-intensity cementite.
2. The hardness of the treated layers is drastically increased in comparison with the untreated sample. Wear rate and wear volume loss of the hardened is about 2.5 lower that of the initial material. Coefficient of friction almost unchanged even due the fact of increasing roughness of the surface.
3. Plasma electrolytic hardening process enhances tribomechanical behavior of 20Cr2Ni4A steel. So, this process and material could be used in the high-speed and heavy-duty gears manufacturing.

Conflicts of interest

The authors declare no conflicts of interest.

Acknowledgments

This work was supported by the grant financing of scientific research for 2018–2020 of Committee of Science of the Ministry of Education and Science of the Republic of Kazakhstan (BR05236748).

REFERENCES

[1] Machinery component maintenance and repair, Elsevier; 2019. https://doi.org/10.1016/C2018-0-04278-4.
[2] Özbek YY. Surface properties of AISI 4140 steel modified by pulse plasma technique. J Mater Res Technol 2020;9:2176–85, http://dx.doi.org/10.1016/j.jmrt.2019.12.048.
[3] Yerokhin AL, Nie X, Leyland A, Matthews A, Dowey SJ. Plasma electrolysis for surface engineering. Surf Coat Technol 1999;122:73–93, http://dx.doi.org/10.1016/S0257-8972(99)00441-7.
[4] Grigoriev S, Metel A, Volosova M, Melnik Y, Ney H, Mustafaev E. Surface hardening of massive steel products in the low-pressure glow discharge plasma. Technologies 2019;7:62, http://dx.doi.org/10.3390/technologies7030062.
[5] Cisquini P, Ramos SV, Viana PR, Lins VD, Franco AR Jr, Vieira EA. Effect of the roughness produced by plasma nitrocarburizing on corrosion resistance of AISI 304 austenitic stainless steel. J Mater Res Technol 2019;8:1897–906, http://dx.doi.org/10.1016/j.jmrt.2019.01.006.
[6] Kaouka A, Benarous K. Electrochemical boriding of titanium alloy Ti-6Al-4V. J Mater Res Technol 2019;8:6407–12, http://dx.doi.org/10.1016/j.jmrt.2019.10.024.
[7] Tyurin YN, Pogrebnjak AD. Electric heating using a liquid electrode. Surf Coat Technol 2001;142–144:293–9, http://dx.doi.org/10.1016/S0257-8972(01)01207-5.
[8] Belkin PN, Kusmanov SA. Plasma electrolytic hardening of steels: review. Surf Eng Appl Electrochem 2016;52:531–46, http://dx.doi.org/10.3103/S106837551606003X.
[9] Rakhadilov BK, Satbayeva ZA, Bayatanova LB, Kilyshkanov MK, Kalibayev KA, Kochneva AK. Influence of electrolyte-plasma surface hardening on the structure and properties of steel 40KhN. J Phys Conf Ser 2019;1393:012119, http://dx.doi.org/10.1088/1742-6596/1393/1/012119.
[10] Zhurerova LG, Rakhadilov BK, Popova NA, Kylyshkanov MK, Buranich VV, Pogrebnjak AD. Effect of the PEN/C surface layer modification on the microstructure, mechanical and tribological properties of the 30CrMnSiA mild-carbon steel. J Mater Res Technol 2020;9:291–300, http://dx.doi.org/10.1016/j.jmrt.2019.10.057.
[11] Belkin PN, Kusmanov SA, Smirnov AA. Plasma electrolytic hardening and nitrohardening of medium carbon steels. Mater Sci Forum 2016;844:146–52, http://dx.doi.org/10.4028/www.scientific.net/MSF.844.146.
[12] Liu K, Yang B, Mo J, Huang H, Wang Q, Zhu X. Application of carburization/induction heat treatment for 20Cr2Ni4A steel. Jinshu Rechuli 2018;43:220–2, http://dx.doi.org/10.13251/j.issn.0254-6051.2018.04.044.
[13] Dayanç A, Karaca B, Kumruoğlu LC. The cathodic electrolytic plasma hardening of steel and cast iron based automotive camshafts. Acta Phys Pol A 2017;131:374–9, http://dx.doi.org/10.12693/APhysPolA.131.374.
[14] Astashchenko VI, Purtova EV. New technology of hardening of chromium-nickel steel parts. Solid State Phenom 2018;284:1221–5, http://dx.doi.org/10.4028/www.scientific.net/SSP.284.1221.
[15] Wang W, Zhao J, Zhai RX, Ma R. Arrhenius-type constitutive model and dynamic recrystallization behavior of 20Cr2Ni4A alloy carburizing steel. Steel Res Int 2017;88:1600196, http://dx.doi.org/10.1002/srin.201600196.
[16] Algahtani A, Mahmoud ERI. Erosion and corrosion resistance of plasma electrolytic oxidized 6082 aluminum alloy surface at low and high temperatures. J Mater Res Technol 2019;8:2699–709, http://dx.doi.org/10.1016/j.jmrt.2019.02.017.
[17] Thermochemical surface engineering of steels, Elsevier; 2015. https://doi.org/10.1016/C2013-0-16318-0.
[18] G02 Committee, Test method for linearly reciprocating ball-on-flat sliding wear; n.d. https://doi.org/10.1520/G0133-05R16.
[19] Kusmanov SA, Kusmanova YV, Naumov AR, Belkin PN. Features of anode plasma electrolytic nitrocarburising of low carbon steel. Surf Coat Technol 2015;272:149–57, http://dx.doi.org/10.1016/j.surfcoat.2015.04.011.
[20] Jiang Y, Geng T, Bao Y, Zhu Y. Electrolyte-electrode interface and surface characterization of plasma electrolytic nitrocarburizing. Surf Coat Technol 2013;216:232–6, http://dx.doi.org/10.1016/j.surfcoat.2012.11.050.
[21] Kashapov RN, Kashapov LN, Kashapov NF. Research of plasma-electrolyte discharge in the processes of obtaining metallic powders. J Phys Conf Ser 2017;927:012086, http://dx.doi.org/10.1088/1742-6596/927/1/012086.
[22] Clyne TW, Troughton SC. A review of recent work on discharge characteristics during plasma electrolytic oxidation of various metals. Int Mater Rev 2019;64:127–62, http://dx.doi.org/10.1080/09506608.2018.1466492.
[23] Pogrebnyak AD, Kaverina AS, Kylyshkanov MK. Electrolytic plasma processing for plating coatings and treating metals and alloys. Prot Met Phys Chem Surf 2014;50:72–87, http://dx.doi.org/10.1134/S2070205114010092.
[24] Huang J, Fan X, Xiong D, Li J, Zhu H, Huang M. Characterization and one-step synthesis of

Hydroxyapatite-Ti(C,N)-TiO_2 composite coating by cathodic plasma electrolytic saturation and accompanying electrochemical deposition on titanium alloy. Surf Coat Technol 2017;324:463–70, http://dx.doi.org/10.1016/j.surfcoat.2017.06.010.

[25] Jiang Y, Bao Y, Yang K. Effect of C/N concentration fluctuation on formation of plasma electrolytic carbonitriding coating on Q235. J Iron Steel Res Int 2012;19:39–45, http://dx.doi.org/10.1016/S1006-706X(13)60018-7.

[26] Mohsenzadeh MS, Mazinani M. On the yield point phenomenon in low-carbon steels with ferrite-cementite microstructure. Mater Sci Eng A 2016;673:193–203, http://dx.doi.org/10.1016/j.msea.2016.07.033.

[27] Li L, Zhang GZ, Fu ZY, Li T, Liu JJ, Tian ZY. Wear mechanisms analysis of material 20Cr2Ni4A. Adv Mater Res 2013;830:13–6, http://dx.doi.org/10.4028/www.scientific.net/AMR.830.13.

[28] Shadrin SY, Belkin PN, Tambovskiy IV, Kusmanov SA. Physical features of anodic plasma electrolytic carburising of low-carbon steels. Plasma Chem Plasma Process 2020;40:549–70, http://dx.doi.org/10.1007/s11090-020-10062-6.

[29] Kanayev AT, Bogomolov AV, Kanayev AA. Increase of wear resistance and contact-fatigue strength of wheel steel by plasma hardening. Solid State Phenom 2018;284:1144–50, http://dx.doi.org/10.4028/www.scientific.net/SSP.284.1144.

[30] Ayday A, Durman M. Wear performance of ductile iron after electrolytic plasma hardening. Met Mater 2019;57:19–26, http://dx.doi.org/10.4149/km_2019_1_19.